Comparison of Imazalil Removal onto Montmorillonite and Nanomontmorillonite and Adsorption Surface Sites Involved: An Approach for Agricultural Wastewater Treatment

Martina Gamba,[†] Federico M. Flores,[†] Jana Madejová,[‡] and Rosa M. Torres Sánchez*,[†]

[†]CETMIC−CCT La Plata, CICBA. Camino Centenario y 506, 1897 M. B. Gonnet, La Plata, Argentina
[‡]Institute of Inorganic Chemistry, Slovak Academy of Sciences, Dúbravská cesta 9, 845 36 Bratislava, Slovakia

ⓢ *Supporting Information*

ABSTRACT: To remove fungicide Imazalil (IMZ) (commercial formulation) from agricultural wastewater, adsorption was performed and compared among montmorillonite (Mt) and four organo-Mts (OMts), with different octadecyltrimethylammonium (ODTMA) loadings. The agglomerates size increase of OMts with respect to Mt found encourages the use of the former in agricultural wastewater treatment. Characterization of the OMts adsorbents by powder X-ray diffraction, infrared spectroscopy, and thermogravimetric analyses, indicated that ODTMA was present in the interlayer with different molecular arrangements, a diminution of the thermal stability of the OMts and an increase of ODTMA loading being observed at the same time. Zeta potential measurements showed electric surface charge reversion from negative to positive when the surfactant loading exceeded 100% of the clay cation exchange capacity (CEC). The IMZ adsorption on the raw Mt showed high pH dependence and affinity toward the fungicide, while OMts showed best IMZ adsorption capacity at high IMZ concentrations inversely related with the ODTMA loading. The characterization of IMZ−adsorbed samples indicated that for IMZ−Mt the interaction between IMZH$^+$ and the siloxane surface was electrostatic. For IMZ−OMt samples the presence of new XRD and FTIR peaks suggested different IMZ interlayer arrangements and direct interaction with the surface, respectively. Analysis of zeta potential measurements indicated synergetic effects between the ODTMA and IMZ molecules at the external surface.

INTRODUCTION

The runoff of pesticide effluents into waterways and aquifer systems is an accumulative problem and leads to a persistent, threatening and detrimental deterioration of the survival of aquatic compartments, flora, fauna, and environmental matrix (water and soil).[1,2] In particular, the production of large volumes of wastewaters containing high concentration of fungicides during the postharvest treatments of fruits and vegetables has become a serious point source of the contamination of natural water resources.[3]

IMZ is a systemic fungicide for postharvest use on bananas, citrus, and preplanting seed treatments of barley and wheat. It is classified as "likely to be a carcinogen in humans" by Environmental Protection Agency of USA.[4] It has been detected in packing plants effluents at concentration close to 100 ppm, decreasing to 20 ppm in adjacent surface water systems.[5] The adsorption process is recognized as the most efficient and promising approach in the wastewater treatment processes.[6] Biobeds have been effectively used for the depuration of wastewaters containing IMZ,[7] and more recently, Martin-González et al.[8] showed IMZ adsorption onto different activated carbon to be a favorable and feasible process. Clay minerals as montmorillonite (Mt) are also known as good adsorbents of many contaminants as pesticides[9] and heavy metals.[10] Particularly, for organic contaminants a significant enhancement in the adsorption capacity of alkylamine-intercalated montmorillonite (OMt) was reported.[11] This was attributed to the attachment of long chain alkyl groups that would increase the number of nonpolar sites for more effective interactions with organic molecules. A particle size increase of around 7 times (measured as apparent diameter) of OMts with respect to Mt samples[12] promotes a good separation of OMts from the suspension. So the use of these systems in water remediation applications, where adsorption is the driven mechanism, could be suggested. In this respect, commercial OMts have already been used successfully in the pilot scheme to decontaminate wastewater containing pesticides.[13] However, there is lack of information about the use of both types of adsorbents toward IMZ.

In this study, the IMZ adsorption capacity of octadecyltrimethylammonium (ODTMA)-Mt samples with different organic loading was determined and compared with that of raw Mt. Adsorption experiments were performed using IMZ commercial formulation. The adsorption pH used was that developed naturally by the suspension with the aim of studying technological application in wastewater produced by fruits packing plants in further works. Mt and OMt samples and some IMZ adsorbed samples were characterized by thermogravimetric analyses (TG), powder X-ray diffraction (XRD), Fourier transform infrared (FTIR) spectroscopy, and zeta potential determinations to attain the IMZ adsorption mechanisms and surface sites involved.

■ EXPERIMENTAL SECTION

Materials. A Patagonian (Rio Negro province) montmorillonite sample, provided by Castiglioni Pes and Cia., was used as received and labeled Mt. The isoelectric point (IEP) = 2.7, specific surface area (SSA) = 34.0 m^2/g, total specific surface area (TSSA) = 621 m^2/g. The mineralogy and chemical analysis of Mt were determined in a previous work.[14] XRD and chemical analysis indicated that the sample contained Na-montmorillonite (>99%) with quartz and feldspars as minor phases. The structural formula obtained from the chemical analysis was $[(Si_{3.89}Al_{0.11})(Al_{1.43}Fe^{3+}_{0.28}Mg_{0.30})O_{10}(OH)_2]$-$Na^+_{0.41}$. The cationic exchange capacity (CEC) determined by the Cu-triethylenetetramine method[15] was 0.8250 ± 0.0007 mmol/g clay.

The adsorbate used was a product commercialized as XEDREL 50 by Magan. The active ingredient in this product is IMZ (Figure 1), present in an aqueous suspension at 47.2% w/w, with very low solubility in water.
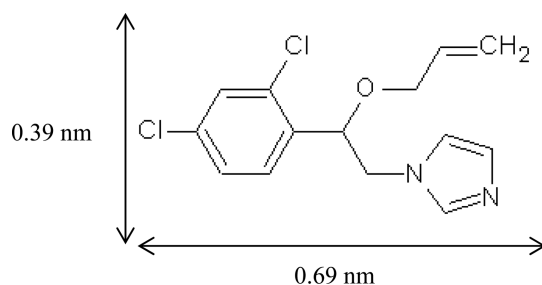
Figure 1. Molecular structure and dimensions of the adsorbate studied, Imazalil.

The IUPAC name of IMZ is (RS)−1-(β-allyloxy-2,4-dichlorophenylethyl) imidazole, its molecular weight (MW) = 297.2 g/mol, pK_a = 6.49, and solubility in water = 0.184 g/L at 20 °C.[16]

Octadecyltrimethylammonium (ODTMA) bromide $[C_{18}H_{37}N(CH_3)_3Br]$ (≥97%), MW = 392.5 g/mol, was purchased from Fluka (Buchs, Switzerland), and used as received. To attain ODTMA-Mts (OMts) samples, the following procedure was performed. A cationic surfactant amount equivalent to 39, 55, 105, and 211% CEC value of Mt was dissolved in 1 L of distilled water at 60 °C, and 10 g of Mt was slowly added. The reaction mixtures were stirred for 2 h at 60 °C. All products were washed with distilled water to free them of bromide anions (tested by $AgNO_3$), dried at 80 °C and ground in an agate mortar. The samples obtained were labeled as OMtX, where X indicated the determined ODTMA loading of the OMts, as percentage of CEC value.

Characterization Methods. Mt and OMts samples and IMZ adsorbed products (labeled as IMZ−Mt or IMZ−OMtX) were analyzed using different techniques.

Carbon analyses were performed using elemental analyzer EMIA 320 V2 AC, HORIBA Jobin Yvon. The average values from three parallel measurements performed for each sample were used.

TG experiments were conducted using a NETZSCH STA 409 PC/PG with alumina as a reference. Samples of 50 mg were placed in Pt crucibles and heated from 30 to 1100 °C at a scanning rate of 10 °C/min in nitrogen/air atmosphere.

XRD patterns (reflection peak $d001$) were collected on powder samples in the range $2° < 2\theta < 15°$ with a counting time of 10 s/step and 0.02° (2θ) step size, using a Philips PW 1710 diffractometer, operated at 40 kV and 30 mA with Cu Kα radiation. The fit quality was controlled by the R^2 value (>0.98).

Electrokinetic potentials were determined using a Brookhaven 90Plus/Bi-MAS with the electrophoretic mobility function. The electrophoretic mobility was converted into a zeta potential value using the Smoluchowski equation. For each determination, 40 mg of sample was dispersed in 40 mL of a 10^{-3} M KCl solution, used as inert electrolyte, and the slurry was stirred. To generate zeta potential versus pH curves, the suspension pH was adjusted using drops of HCl or KOH of different concentrations followed by magnetic stirring until equilibrium was attained (10 min).

Particle size determinations were performed on a 10^{-3} M KCl solution with a 1% w/w particle dispersion by dynamic light scattering (DLS) measurements using the same Brookhaven equipment utilized for zeta potential measurements (multiangle particle sizing function), operating at λ = 635 nm, 15 mW solid state laser, scattering angle = 90°, and temperature = 25 °C. The determination rendered the apparent equivalent sphere diameter, Dapp.

FTIR spectra were collected by a Nicolet 6700 Fourier transform infrared spectrometer from Thermo Scientific. The KBr pressed disk technique (1 mg of sample and 200 mg of KBr) and Smart Diffuse Reflectance Accessory were used to measure the FTIR spectra in the mid-infrared (MIR, 4000−400 cm^{-1}) and near-infrared (NIR, 12000−4000 cm^{-1}) regions, respectively. Spectra were obtained by coaddition of 64 scans at a resolution of 4 cm^{-1}. Spectra manipulations were performed using the Thermo Scientific OMNIC software package.

IMZ Adsorption Studies. A weighed amount of the commercial fungicide was dissolved in pure ethanol in order to prepare a concentrated solution (5000 mg/L) and additional concentrations were obtained by dilution in distilled water. Kinetic studies (Supporting Information, Figure S1) indicated that the contact time to reach equilibrium was 1 h for Mt and 7 h for OMt137 sample. The adsorption experiments were accomplished with a contact time of 24 h, at 20 °C, under stirring, to ensure that the equilibrium was reached in all adsorption systems. Batch adsorption experiments were performed with an adsorbent/adsorbate ratio of 1 mg/mL, using an IMZ concentration range from 10 to 600 mg/L. The pH of all adsorption isotherms was achieved naturally within pH = 6.8−8.5 and 6.8−7.5 for Mt and OMts samples, respectively. Also the IMZ adsorption isotherm on Mt at pH = 7 was obtained by adjusting the pH of the initial IMZ solution and later that of the obtained suspension to pH 7.0, using drops of HCl or KOH of different concentrations. Blanks of IMZ solution and adsorbate suspensions were run for each experiment to evaluate adsorbate and adsorbent stability. After the equilibration time the suspensions were centrifuged at 14 000 rpm during 15 min. The solid phases corresponding to the highest IMZ initial concentration studied (600 ppm) were rinsed with distilled water, air-dried, and stored for further analysis. The concentration of IMZ in the supernatants was analyzed by high performance liquid chromatography (HPLC) coupled with UV−visible detection (λ = 220 and 272 nm) using a Shimadzu HPLC C18 column (4.6 mm × 250 mm, 4.6 μm). Mobile phase was 80/20 methanol/water mixture flowing at 1 mL/min. The injected volume was 20 μL. The linear range of IMZ concentrations was within 3−800 mg/L (R^2 = 0.999). The amount of adsorbed IMZ, Q, (mg IMZ/g adsorbent) was

Table 1. Carbon Content Referred as ODTMA Loading (% CEC)[a] and Thermo-analytical Characteristics of Surfactant and Clays

sample	ODTMA added (% CEC)	ODTMA loading (% CEC)	water content (%)	desurfactant temperature (°C)	Dapp (nm)
ODTMA	na	na	0	249.4	na
Mt	na	na	22.4	na	674 ± 51
OMt39	39	38.89	2.5	289.9	1730 ± 32
OMt55	55	54.70	1.9	291.4	2399 ± 38
OMt75	105	74.73	1.8	290.0	2802 ± 53
OMt137	211	137.13	1.3	263.5	8351 ± 46

[a]na: not applicable.
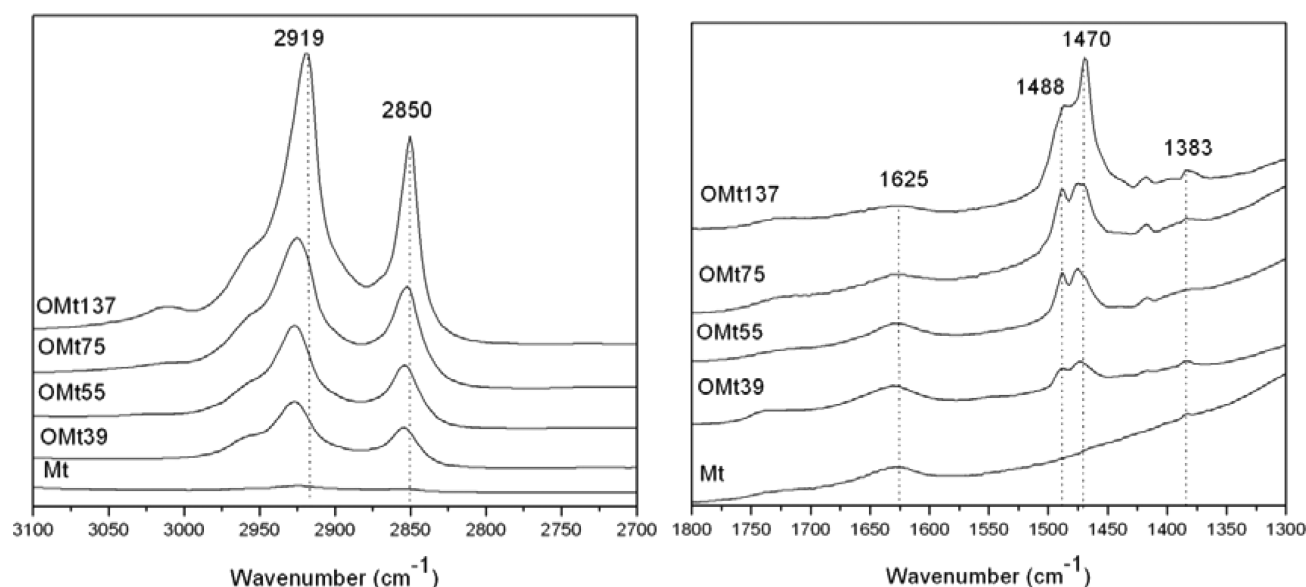
Figure 2. MIR spectra of Mt and OMts indicated samples.

determined as the difference between the initial IMZ concentration (C_i) and that at equilibrium (C_f).

The Langmuir and Freundlich models, used to adjust the experimental isotherms are given by eqs 1 and 2, respectively.

$$Q = Q_{max}kC_f/(1 + kC_f) \tag{1}$$

$$Q = K_F \cdot C_f^{(1/n)} \tag{2}$$

In eq 1, Q_{max} is the maximum amount adsorbed within a monolayer (mg/g) and k (L/mg) is the Langmuir dissociation constant, which is related to the adsorption energy. The Langmuir isotherm model assumes a monolayer adsorption on a surface with a finite number of identical sites, where all sites are energetically equivalent and without interaction between adsorbed molecules.

In the Freundlich equation (eq 2), K_F (L/g) indicates adsorption capacity, and $1/n$ (dimensionless) indicates the variation in adsorption as a function of concentration.[17] Freundlich expression is an empirical equation based on the adsorption on a heterogeneous surface.

■ RESULTS AND DISCUSSION

Adsorbents Characterization. *Carbon Content Analyses.* Xu and Boyd[18] proposed a model to explain hexadecyltrimethylammonium (HDTMA) adsorption onto Na+-smectite. They showed that at HDTMA loadings lower than 75% CEC, HDTMA adsorption was via cation exchange, but when HDTMA loadings were higher than that value,

HDTMA adsorption via cation exchange approached its maximum and HDTMA adsorption via van der Waals interactions occurred. Carbon content analyses (Table 1) suggested that this model is also valid for ODTMA adsorption onto Mt. When the ODTMA added amount was lower than 100% CEC, all the surfactant cations were loaded through the cationic exchange (OMt39 and OMt55 samples). When the ODTMA added was 105% CEC only 75% CEC was loaded through ion exchange and the excess remained in the solution (OMt75). Finally, when the added amount was up to two times the CEC value, all inorganic cations were exchanged and the excess surfactant was adsorbed via van der Waals interactions (OMt137, Table 1).[18,19]

FTIR Spectroscopy. In addition to absorption bands related to stretching and bending vibrations of the Mt structural groups (νOH at 3630 cm^{-1}; νSiO at 1045 cm^{-1}; δAlAlOH at 918 cm^{-1}; δAlMgOH at 844 cm^{-1}; δAlOSi at 525 cm^{-1}; δSiOSi at 460 cm^{-1}), C−H stretching and bending vibrations of ODTMA occurred in the MIR spectra of OMts (Figure 2 and Supporting Information, Table S1). The absorption bands around 2920 and 2850 cm^{-1} corresponded to asymmetric and symmetric stretching vibrations of CH$_2$ groups, respectively. The intensity of the bands increased with ODTMA loading, and their positions decreased from 2927 and 2855 cm^{-1} for OMt39 to 2919 and 2850 cm^{-1} for OMt137. This behavior indicated that alkyl chains adopted more ordered structure as the ODTMA loading increased[20,21] (alkyl chain conformations in the interlayer space will be further discussed in the XRD section).

The appearance of bending vibration of the alkyl chains ($\delta_{as}CH_3-N$ at 1488 cm^{-1}; $\delta_{as}CH_2$ at 1470 cm^{-1}; $\delta_{as}CH$ at 1417 cm^{-1} and δ_sCH_3 at 1383 cm^{-1}) also verified the intercalation of surfactant cations. The band at about 1625 cm^{-1} corresponded to OH deformation of water in all the samples and its intensity was weaker for OMts than for Mt[22] (Figure 2).

The NIR spectroscopy provides structural information often not available from the MIR region.[23] The NIR spectra of Mt and OMts are given in Figure 3 and the interpretation of the individual vibration modes for Mt and OMt39, OMt55 samples are summarized in Supporting Information, Table S2.
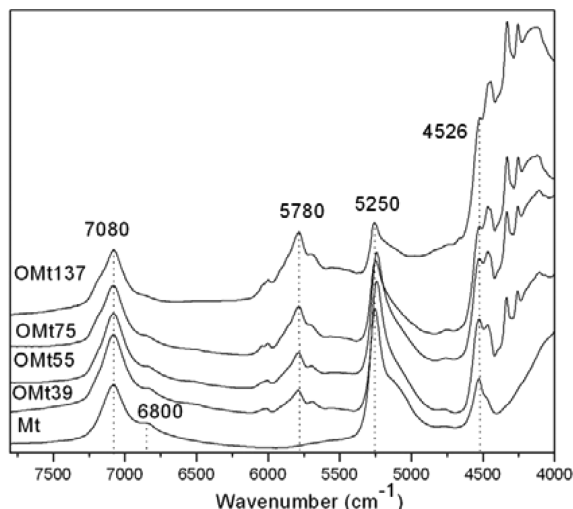
Figure 3. NIR spectra of Mt and OMts indicated samples.

For all samples, the intense bands at ~7080 and 5250 cm^{-1} were seen (Figure 3). The first one was assigned to overlapping contributions of the OH stretching overtones (2ν) of structural OH groups and weakly hydrogen-bonded H_2O molecules, while the second one was attributed to ($\nu + \delta$) H_2O.[24,25] The shoulder near 6848 cm^{-1} (better resolved for Mt than OMts samples) was due to the first overtone of water molecules involved in strong hydrogen bonds.[23] The interlayer entrance of ODTMA cations produced the appearance of new bands due to CH_2 and CH_3-N stretching overtones (6200−5300 cm^{-1}) and combinations (4800−4000 cm^{-1}).

XRD Patterns. The surfactant incorporation in the Mt interlayer space can also be followed through the shift of the basal reflection ($d001$). Figure 4 showed that for all OMts samples the peak shifted to lower angle (2θ) with respect to that of the Mt sample. The interlayer spaces thicknesses of the OMts samples were determined from the difference between the $d001$ value and that of dehydrated Mt (0.97 nm).[26] The calculated interlayer space for the OMt39 sample of 0.46 nm corresponded to a lateral monolayer arrangement of the surfactant.[27] For OMt55 sample a peak enlargement was observed. Its deconvolution (Figure 4 inset) indicated two calculated interlayer thicknesses of 0.69 and 0.50 nm, which could be assigned to a transition of surfactant arrangements from lateral monolayer to lateral bilayer. The reflection peak observed for OMt75 sample indicated an interlayer thickness of 0.82 nm, assigned to lateral bilayer arrangement of the surfactant. Summarizing, when the ODTMA loading was up to 75% CEC, the alkyl chains were parallel to the clay surface. Zanini et al.[28] observed similar space thicknesses for the benzalkonium chloride (BAC) molecules with alkyl chains
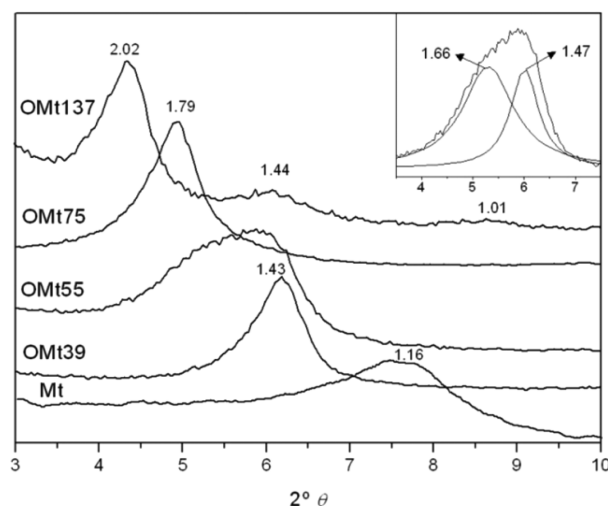

Figure 4. XRD patterns of Mt and OMts indicated samples. Inset: Deconvolution peaks of OMt55. Basal spacing values are expressed in nm.

having 12 or 14 carbon atoms, at loadings lower than 80% CEC. The flat orientation explains the independence of $d001$ values with the chain length for BAC (12 or 14 carbon atoms) and ODTMA (18 carbon atoms). For the OMt137 sample, as van der Waals interactions occurred, a multiphase system with both regularly and randomly intercalated layers was obtained. Three peaks, corresponding to 1.05, 0.47, and 0.04 nm of layer thickness, were observed. The first one was assigned to the pseudotrilayer or paraffin-like monomolecular arrangements;[29] the second one was assigned to the lateral monolayer array. The last one could come from partially collapsed layers generated by the surfactant entrance and concurrent remotion of inorganic ions with its hydration sphere.[12,30]

Zeta Potential Data and Dapp Measurements. Zeta potential measurements reflect the electrical charge on the external surface.[31] Figure 5 showed zeta potential vs pH curves for Mt and OMts samples. The Mt sample depicted a pH-independent zeta potential behavior (at around −30 mV) over a wide pH range (from pH 2 to 8) originated by a constant
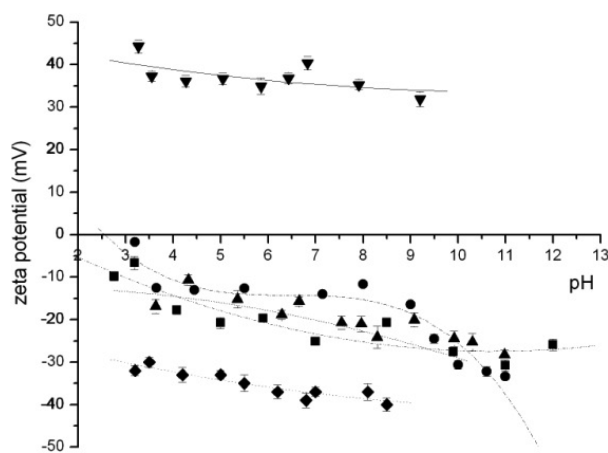
Figure 5. Zeta potential vs pH curves of all samples: (♦) Mt; (●) OMt39; (■) OMt55; (▲) OMt75; and (▼) OMt137. The fitting lines are a linear regression using a polynomial curve. Lines located on the graph are to assist viewing the curve taking into account the data dispersion.
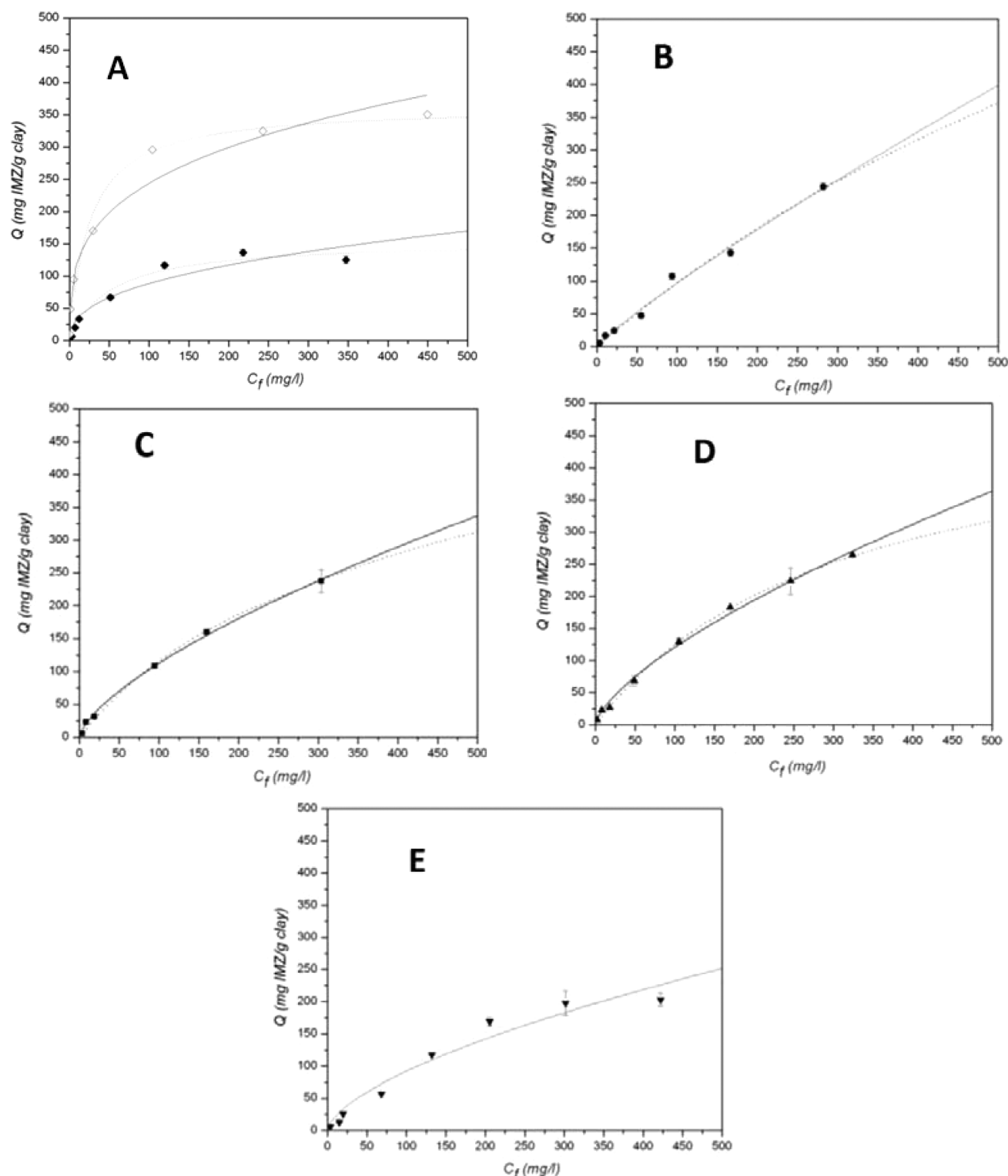
Figure 6. Adsorption isotherms of IMZ on (A) Mt without (◆) and with (◇) pH adjustment at pH = 7.0, (B) OMt39, (C) OMt55, (D) OMt75, and (E) OMt137 samples. Lines indicated (——) Freundlich and (····) Langmuir fits.

surface potential (structure or basal sites) and variable charge (edge sites). As a result of adjustments between the Stern layer and the diffuse layer, the potential is kept constant leading to a flat curve, similar to that published in the literature.[31,32] No significant differences among zeta potential curves of the OMt39, OMt55, and OMt75 samples were observed with values less negative than those of the Mt sample over the pH

range studied. In contrast, a reversal surface electric charge was found for the OMt137 sample. These results suggested that little ODTMA amounts were bonded to the external surface until the amount that exceeded the 100% CEC was intercalated (Figure 5).[18] As was confirmed recently by Pecini and Avena,[33] Mt structural charges were neutralized at loadings of different cationic dyes very close to the CEC value, the further loadings

of cationic molecules were governed by the charging behavior of the edge surfaces of the particles. The positive surface electric charge found for the OMt137 sample, with surfactant loading above the CEC, agreed with that behavior and indicated that the surfactant covered the edges and external surface in bilayer arrangements[34] with some positive ammonium groups oriented out of the surface.[12]

A consequence of electric charge changes is the enlargement of OMts aggregates with respect to that of Mt (measured as Dapp, Table 1) in agreement with data found by Bianchi et al.[12] Samples with ODTMA content lower than 100% of the CEC value (OMt39, OMt55, and OMt75) presented Dapp values that were up to four times bigger than that of Mt. The sample with highest ODTMA loading (OMt137), which also showed electric charge reversal on the external surface, showed the highest Dapp value, going up to 8350 nm, most probably due to micelle formation on the OMt137 sample surface (Table 1).

TG and Derivative-TG Analyses. TG analyses (Figure S2) indicated several mass-loss steps: The mass loss before 200 °C was attributed to the dehydration of physically adsorbed water and water molecules around metal cations on exchangeable sites in Mt.[35] The water content in OMts was lower than in Mt (22.5%) and decreased from OMt39 to OMt137, due to the increasing hydrophobicity of the samples (Table 1) as indicated in the FTIR section. The mass loss occurring from 200 to 400 °C was attributed to the decomposition of the surfactant. The desurfactant temperature, obtained from derivative-TG (DTG) curves, was between 289.9 to 291.4 °C for OMt39, OMt55, and OMt75 and decreased to 263.4 °C for OMt137, moving closer to the pure surfactant decomposition temperature (249.4 °C, Table 1 and Supporting Information, Figure S2). As suggested previously[36,37] thermal stability of organoclays decreased with increasing loading of surfactant. Finally, the mass-loss over the temperature from 500 to 800 °C was ascribed to the loss of the structural OH units of the montmorillonite (Supporting Information, Figure S2).
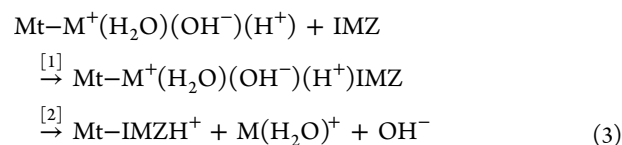
IMZ Adsorption Isotherms. The obtained isotherms of IMZ with their corresponding Freundlich and Langmuir fits are shown in Figure 6 for all samples. Particularly, the IMZ adsorption on the Mt sample (Figure 6A) without and with pH adjustment at pH 7.0 was compared, while the isotherms for the OMts samples (Figure 6B to 6E) were obtained without pH adjustments.

The fit correlation coefficients (R^2) and the adjustment parameters obtained from Freundlich and Langmuir equations are shown in Table 2. According to the R^2 term, the experimental data were appropriately described by both models for all the samples. To simplify the analysis, the IMZ–

adsorption mechanism was explained in terms of Langmuir assumptions.

Table 2 indicated that OMts samples had better Q_{max} than those obtained by Mt sample without pH adjustment. Although Q_{max} values are an extrapolation because experimental data does not allow obtaining a plateau, it is a good parameter to compare the performance of the adsorbents. A deeper observation of the adsorption isotherms (Figure 6) allowed differentiating two behaviors within the IMZ concentration range analyzed for Mt and OMts samples. When the IMZ concentration was less than 50 ppm, the Mt sample revealed higher affinity than the OMts ones, indicated by the initial slope of the curve and reflected in higher k values. In contrast, for IMZ concentrations between 50 and 600 ppm, OMts were better adsorbents than the Mt sample without pH adjustment, reaching higher Q_{max} values. In agreement with this behavior, the adsorption dependence on concentration among samples (Table 2) was evidenced by the decrease of Freundlich's $1/n$ parameter. All OMt samples achieved higher Q_{max} values than that indicated for activated carbons used as adsorbents, although activated carbons achieved larger BET surface and pore volume (1300−1469 m^2/g and 0.59−1.2 m3/g, respectively)[8] than organoclays (BET surface of 8.8−23 m^2/g and pore volume between 0.06 and 0.08 m^3/g).[38]

Socías-Viciana et al.[39] found similar concentration dependence for the prometrone adsorption (a nonselective herbicide, with weak basic character), on two reference smectites. Their results were explained on the basis of the hydrophobicity and basic character of the herbicide,[40] and resumed by eq 3 valid also for IMZ adsorption:

$$\text{Mt}-\text{M}^+(\text{H}_2\text{O})(\text{OH}^-)(\text{H}^+) + \text{IMZ}$$
$$\overset{[1]}{\rightarrow} \text{Mt}-\text{M}^+(\text{H}_2\text{O})(\text{OH}^-)(\text{H}^+)\text{IMZ}$$
$$\overset{[2]}{\rightarrow} \text{Mt}-\text{IMZH}^+ + \text{M}(\text{H}_2\text{O})^+ + \text{OH}^- \qquad (3)$$

where M$^+$ represents an exchangeable inorganic cation. First, neutral IMZ is adsorbed on the hydrophobic part of the clay (reaction 1, eq 3).[41−43] In a second step, the polarized water molecules associated with the exchangeable inorganic cations promote imidazole ring protonation (reaction 2, eq 3) which is thus adsorbed in the interlayer of Mt. Since more than 90% of the total surface of Mt corresponds to the internal surface, the above-described mechanism is appropriate to explain the observed behavior.

For the Mt sample, as IMZ concentration increased, the pH of the suspension increased too (from 6.8 to 8.5) due to the basic character of the fungicide and protonation of the imidazol group (=N−H group) at the clay surface. At alkaline pH the surface Si−OH groups are fully or partially deprotonated, resulting in a decrease of the adsorption capacity of Mt due to the inhibition of the mechanism described by eq 3. Furthermore, when the pH was maintained at a neutral value, an increase on the adsorption was observed (Figure 6A) reaching a Q_{max} value of 363 mg/g (R^2 (Langmuir) = 0.978), which is 2.34 times bigger than that attained by the same sample without pH adjustment.

For OMts samples, there was an enhancement of IMZ adsorption inversely related to the ODTMA loading (Figure 6B to 6E and Table 2) in agreement with that found by Zhang et al.[44] for mixed cationic−nonionic surfactants.

Generally, the mechanism proposed for the adsorption of organic compounds onto organoclays samples involves (1)

Table 2. Parameters of the Freundlich and Langmuir Models Fitted to the Experimental Adsorption Data

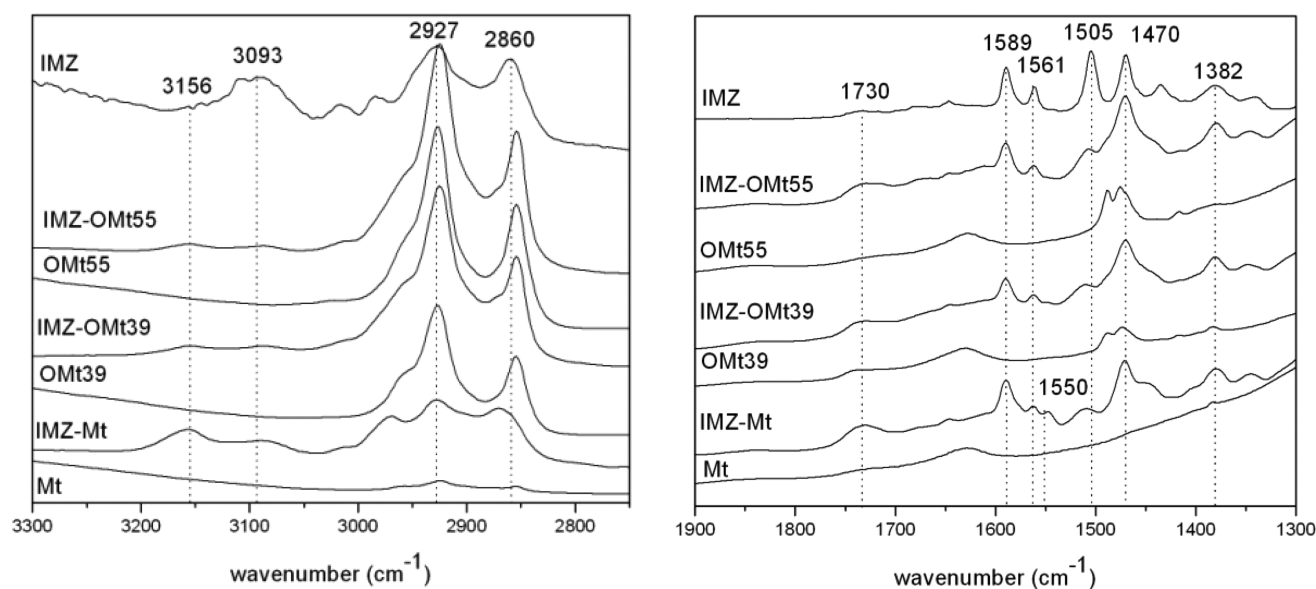| | Freundlich equation | | | Langmuir equation | | |
| | $Q = K_F C_f^{(1/n)}$ | | | $Q = Q_{max} k C_f/(1 + k C_f)$ | | |
sample	K_F	$1/n$	R^2	Q_{max}	k (10^{-3})	R^2
Mt	13.634	0.399	0.925	155	20.53	0.976
Mt (pH = 7)	62.236	0.296	0.959	363	40.37	0.978
OMt39	1.672	0.881	0.990	1267	0.84	0.983
OMt55	4.911	0.681	0.998	597	2.22	0.982
OMt75	5.143	0.685	0.991	514	3.22	0.998
OMt137	5.144	0.399	0.960	348	3.92	0.991

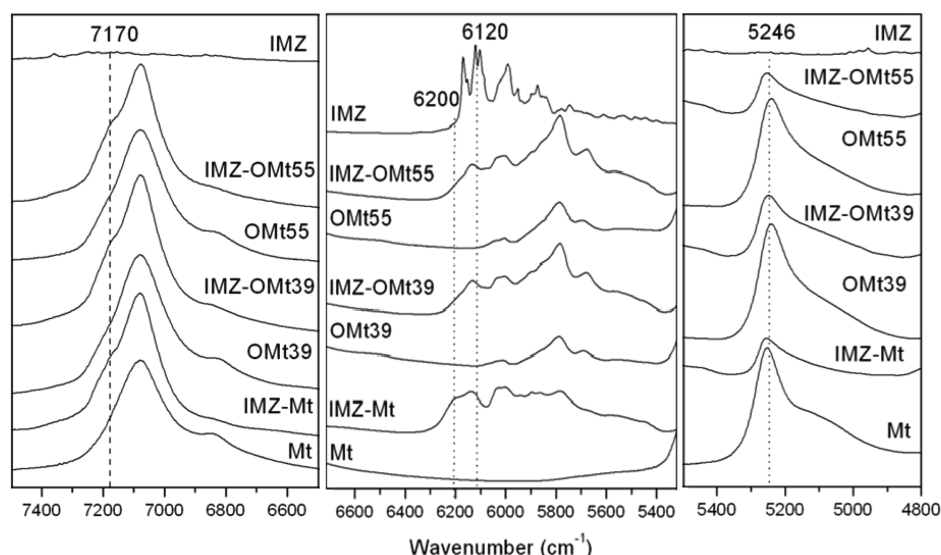**Figure 7.** MIR spectra of IMZ and IMZ−adsorbed samples.

Figure 8. NIR spectra of IMZ and IMZ−adsorbed samples.

organophilic partitioning, (2) electrostatic interaction, and (3) chemical adsorption between the adsorbate and the adsorbent.[45] Because the IMZ exists in equilibrium with its cationic form (pK_a = 6.49) the three processes could influence the removal of IMZ by OMts. As the pH of the adsorption isotherm suspensions was between 6.8 and 7.5 for all OMts samples, the neutral form of IMZ would be the main specie and the organophilic partitioning would be the dominant mechanism. If the above state were true, the IMZ adsorption capacity should be enhanced with the increasing of ODTMA loading; however, the opposite behavior was found (Figure 6).

A way to rationalize this observation was proposed by Jaynes and Boyd,[42] who suggested that exchanged organic cations were not directly involved in the adsorption of aromatic compounds from water by organo-smectites. It was proposed that the organic cations would only have function as "pillars" to keep the interlayers apart. Furthermore, the siloxane surface of the clay appeared to be the actual adsorptive surface for the adsorbent. In OMts, the exchanged ODTMA cations would

displace the hydrophilic, inorganic exchangeable cations enabling hydrophobic IMZ molecules to interact directly with the hydrophobic siloxane surfaces. When the amount of exchanged ODTMA was 39 or 55% CEC, the interlayer clay surface was available as adsorption sites,[42] while for OMt137, almost all the internal and external surface was covered by the alkyl chains of ODTMA.

In this sense Socías-Viciana[39] reported a compromise between the organic interlayer width and the interlayer room available for the sorption of the herbicide prometrone onto different organoclays. According to our observations and in line with the above-described models, the presence of ODTMA seems to be necessary to change the environment of the Mt surface and to keep the interlayers open.

Another effect may be involved in the IMZ adsorption by OMt137. As IMZ exists in equilibrium with its cationic form, electrostatic repulsion between IMZH+ and the positively charged surface of OMt137 would further diminish its adsorption capacity. This effect would not be present on

Table 3. IMZ and IMZ Adsorbed Samples (C_i = 600 ppm): Basal Spacing, Organic Decomposition, and Zeta Potential Values (pH = 7)^a

sample	basal spacing (nm)	desurfactant temperature (°C)	IMZ—decomposition temperature (°C)	zeta potential (mV)
IMZ	na	na	282.3	na
IMZ—Mt	1.82	na	293	−18.4 ± 0.61
IMZ—OMt39	1.75	265	308	−17.49 ± 0.57
IMZ—OMt55	3.22	262	312	−28.09 ± 0.72
IMZ—OMt75	3.13	262	314	−19.20 ± 0.83
IMZ—OMt137	3.50	260	303 (shoulder)	19.07 ± 0.98

^{a}na, not applicable; nd, not determined ($2°\theta < 2$).

OMt39, OMt55, and OMt75 due to their negative surface charge (Figure 5). These electrostatic behaviors will be discussed more deeply with the analysis of IMZ adsorbed samples by zeta potential measurements in further paragraphs.

Characterization of Adsorbed Products. FTIR spectroscopy provided information about the structural changes that occurred after IMZ adsorption and confirmed the mechanisms proposed in previous sections. IMZ MIR and NIR spectra are shown in Figures 7 and 8, respectively. In the MIR spectrum the bands due to CH stretching vibrations of aliphatic, vinylic, and aromatic groups occurred in the 3600−2600 cm^{-1} region. The bands in the 1800−1380 cm^{-1} region were assigned to vinylic and aromatic CC stretching vibrations, and the vibrations attributed to CH bending vibration appeared in the 1380−500 cm^{-1} region (Supporting Information, Table S1). The NIR spectrum of IMZ showed the bands in the 6200−5700 cm^{-1} region corresponding to the first overtone of aliphatic, vinylic, and aromatic CH stretching vibration, while the combinations of aromatic CH and CC stretching modes appeared in the 4600−4400 cm^{-1} region. Finally, the bands below 4400 cm^{-1} were assigned to CH combination modes (Supporting Information, Table S2).

After IMZ adsorption on Mt the characteristic bands of both IMZ and Mt appeared in the MIR spectrum of the IMZ−Mt sample. The vibrational modes at 3089, 2928, 2871, 1590, 1471, and 1380 cm^{-1} were assigned to IMZ (Supporting Information, Table S1). The imidazole ring protonation, proposed in the IMZ adsorption isotherms section to explain IMZ adsorption on the Mt sample, was confirmed by the appearance of new bands at 3155 and 1550 cm^{-1} in the IMZ−Mt spectrum. These bands, assigned to NH$^+$ stretching and bending vibrations, respectively, are characteristic for pyridine protonation and can be used as evidence of the presence of acid sites in clay minerals.[46] A significant decrease of νNH$^+$ and δNH$^+$ peaks intensities in OMts spectra could be due to the diminution of the water amount in hydrophobic OMts (Table 1). Moreover, a stronger C=C (Ar) band near 1560 cm^{-1} can partly overlap the NH$^+$ bending band. Furthermore, the band at 6200 cm^{-1} in the NIR spectrum of IMZ−Mt (Figure 8) was assigned to the first overtone of the NH$^+$ stretching mode and also confirmed the imidazole protonation.

Although the recognition of IMZ bands in the MIR spectra of IMZ−OMts was less straightforward due to overlapping with ODTMA vibrations, the peaks at 3090, 1590, 1562, 1381, and 1287 cm^{-1} confirmed its adsorption on OMts (Figure 7 and Supporting Information, Table S1). No differences on the shapes and positions of the bands due to ODTMA vibration after IMZ adsorption (Figure 7, Table S1) confirmed that ODTMA was not directly involved in the bond with IMZ. In contrast, changes in the 7080 cm^{-1} band shape for all adsorbents were observed. While the NIR spectrum of IMZ showed no bands in this region, a new 2νOH component near 7170 cm^{-1} appeared for all IMZ adsorbed samples (Figure 8) because of a change in the environment of the structural OH groups. These results indicated that the actual adsorbent surface for IMZ adsorption was a siloxane surface of montmorillonite while ODTMA cations acted only as "pillars" keeping the interlayers apart and enabling the IMZ to interact directly with the hydrophobic tetrahedral sheets. The position and relative intensity of the ($\nu + \delta$) H$_2$O band was also modified after IMZ adsorption (Figure 8, Table 2). In all cases, a higher position of this peak indicated weaker H-bonds between water and the Mt surface. In addition, the intensity of this band significantly decreased after IMZ adsorption indicating an increase in hydrophobicity of IMZ−Mt and IMZ−OMt.[23]

The adsorption of IMZ on the Mt surface modified also the position of the first CH overtone of the vinyl group. While for pure IMZ the band was observed at 6120 cm^{-1}, the NIR spectra of IMZ−Mt and IMZ−OMt samples showed a shift to 6130 cm^{-1} (Figure 8). Most probably, the shift resulted from the interactions between the vinyl group and the adsorbents.

Finally, another process may have occurred during IMZ adsorption. A new band at ~1730 cm^{-1} appeared for all IMZ samples spectra (Figure 7). The only functional group that absorbs the infrared radiation in this region is the carbonyl group (C=O). To explain the appearance of it in the system, it is suggested that some IMZ molecules are metabolized to imazalil ethanol[47] and the OH group of the metabolite is further oxidized to the carbonyl group.

The XRD patterns of IMZ adsorbed samples (Table 3) indicated an increase of the basal spacing compared with the respective starting materials (Figure 4) pointing out the importance of the interlayer sites for the IMZ adsorption. The basal spacing of Mt sample was expanded by 0.66 nm upon IMZ adsorption (Table 3). However, if a dehydrated Mt was considered with d001 = 0.97 nm,[26] the recalculated increase of basal space by IMZ entrance was 0.85 nm. Determination of the IMZ molecule dimensions by computational calculations indicated the following dimensions: 0.69 nm large and 0.39 nm high (Figure 1). These results must be taken only as an approximation to the true molecular dimensions because a tridimensional conformation was not taken into account. Notwithstanding, it allowed the suggestion that IMZ produced the 0.85 nm interlayer expansion with release of inorganic interlayer cations (eq 3). IMZ−OMt samples also showed basal spacing increases, from 0.32 to 1.48 nm for OMt39 and OMt137 (Table 3), respectively, indicating that IMZ had penetrated the interlayer space. Different d001 values could be assigned to different amounts or configurations of IMZ in the interlayer space.

DTG analyses revealed that while pure IMZ decomposed at 282 °C, IMZ molecules bonded to the Mt siloxane layer

required a higher temperature to be decomposed[48] (293 °C for IMZ−Mt and around 310 °C for IMZ−OMts). At the same time, the IMZ adsorption onto OMt modified the interaction between ODTMA and clay surface, leading to a weaker bond between them and reducing the "de-surfactant" temperature to around 262 °C (Table 3). As indicated by Zhang et al.,[44] the coadsorption of the surfactant and the fungicide onto clay mineral reduced the thermal stability of the organoclays.

Zeta potential measurements allowed inferring charge changes on the external surface of the adsorbents with IMZ. For the Mt sample a decrease of negative charge was seen (Table 3 and Figure 5), in agreement with the reaction indicated in eq 3. The IMZ−OMt137 sample showed a decrease of positive surface charges from +40 to +19.7 mV (Figure 5, Table 3). As the ODTMA loading exceeded the CEC value, the formation of some mixed IMZ−ODTMA micelles could be attained.[44] This would produce a decrease of the ODTMA packaging at the external surface and explained the lower IMZ adsorption capacity of OMt137 respect to the less loaded OMt samples. For OMt39, OMt55, and OMt75 samples the IMZ adsorption produced a lower increase of negative surface charges, respect to that found for the OMt137 sample, which could also be assigned to the formation of same mixed IMZ−ODTMA micelles on the external surface.

CONCLUSIONS

In the present study, raw clay mineral from the Argentinean Patagonia was converted into hydrophobic organoclays by intercalating different loading amounts of octadecyltrimethylammonium bromide, to test their capacity to remove IMZ from aqueous solutions. As the surfactant loading was increased, different arrangements in the interlayer produced modifications of the Mt basal spacing, surface electric charges, shifts of MIR and NIR bands positions, and also different desurfactant temperatures.

Adsorption experiments showed that the IMZ adsorption capacity was highly dependent on the IMZ initial concentration. On one hand, Mt was the best adsorbent for amounts lower than 50 ppm, explained in terms of the IMZ basic character. On the other hand, OMts samples were better adsorbents than Mt for IMZ concentrations higher than 50 ppm. At the same time, within OMts samples, the increase of the ODTMA content resulted in a diminution of the IMZ adsorption capacity. FTIR analyses indicated that ODTMA did not directly interact with the fungicide, the adsorptive surface being the siloxane surface of the clays. The function of ODTMA was to displace inorganic cations and to keep the interlayer space open to enable IMZ interaction with the hydrophobic tetrahedral surface. Inner and outer surfaces were involved in the IMZ adsorption onto all the samples, producing changes in XRD pattern and zeta potential values, respectively.

This study evidenced a better adsorption of IMZ onto OMt with respect to Mt and activated carbons, at concentrations found in packing plants wastewater. These results and the large agglomerates size of OMts promote the potential application of OMts as adsorbents for environmental pollutants aiming to their feasible separation from the aqueous suspension. However, future studies should attempt to use mixtures of commercial fungicides in use in packing plants to confirm the success of the process.

ASSOCIATED CONTENT

Supporting Information

Kinetic studies of IMZ adsorption onto Mt and OMt137, thermogravimetric and derivative-thermogravimetric studies, wavenumber and assignment of the bands observed in the MIR and NIR spectra of Mt, OMt39, OMt55, IMZ and IMZ-adsorbed samples. This material is available free of charge via the Internet at http://pubs.acs.org.

AUTHOR INFORMATION

Corresponding Author

*E-mail: rosats@cetmic.unlp.edu.ar.

Notes

The authors declare no competing financial interest.

ABBREVIATIONS

Mt = montmorillonite
ODTMA = octadecyltrimethylammonium
OMts = octadecyltrimethylammonium exchanged montmorillonite
OMt39 = octadecyltrimethylammonium 39% CEC exchanged montmorillonite
OMt55 = octadecyltrimethylammonium 55% CEC exchanged montmorillonite
OMt75 = octadecyltrimethylammonium 75%CEC exchanged montmorillonite
OMt137 = octadecyltrimethylammonium 137% CEC exchanged montmorillonite
IMZ = imazalil

REFERENCES

(1) Foo, K. Y.; Hameed, B. H. Detoxification of pesticide waste via activated carbon adsorption process. *J. Hazard. Mater.* 2010, *175*, 1−11.
(2) Hameed, B. H.; Salman, J. M.; Ahmad, A. L. Adsorption isotherm and kinetic modeling of 2,4-D pesticide on activated carbon derived from date stones. *J. Hazard. Mater.* 2009, *163*, 121−126.
(3) Masiá, A.; Campo, J.; Navarro-Ortega, A.; Barceló, D.; Picó, Y. Pesticide monitoring in the basin of Llobregat River (Catalonia, Spain) and comparison with historical data. *Sci. Total Environ.* 2014, *503−504*, 58−68.
(4) *Reregistration eligibility decision for Imazalil Chemical List B Case No. 2325*; *EPA*: Washington, DC, 2003; http://www.epa.gov/oppsrrd1/REDs/2325red_imazalil.pdf.
(5) Castillo, L. E.; Ruepert, C.; Solis, E. Pesticide residues in the aquatic environment of banana plantation: Areas in the north Atlantic zone of Costa Rica. *Environ. Toxicol. Chem.* 2000, *19*, 1942−1950.
(6) Yuen, F. K.; Hameed, B. H. Recent developments in the preparation and regeneration of activated carbons by microwaves. *Adv. Colloid Interface Sci.* 2009, *149*, 19−27.
(7) Omirou, M.; Dalias, P.; Costa, C.; Papastefanou, C.; Dados, A.; Ehaliotis, C.; Karpouzas, D. G. Exploring the potential of biobeds for the depuration of pesticide-contaminated wastewaters from the citrus production chain: Laboratory, column and field studies. *Environ. Pollut.* 2012, *166*, 31−39.
(8) Martín-González, M. A.; González-Díaz, O.; Susial, P.; Araña, J.; Herrera-Melián, J. A.; Doña-Rodríguez, J. M.; Pérez-Peña, J. Reuse of *Phoenix canariensis* palm frond mulch as biosorbent and as precursor of

activated carbons for the adsorption of Imazalil in aqueous phase. *Chem. Eng. J.* **2014**, *245*, 348−358.

(9) Kouras, A.; Zouboulis, A.; Samara, C.; Kouimtzis, T. Removal of pesticides from aqueous solutions by combined physicochemical processes—The behaviour of lindane. *Environ. Pollut.* **1998**, *103*, 193−202.

(10) Lombardi, B.; Baschini, M.; Torres Sánchez, R. M. Bentonite deposits of Northern Patagonia. *Appl. Clay Sci.* **2003**, *22*, 309−312.

(11) Fatimah, I.; Huda, T. Preparation of cetyltrimethylammonium intercalated Indonesian montmorillonite for adsorption of toluene. *Appl. Clay Sci.* **2013**, *74*, 115−120.

(12) Bianchi, A. E.; Fernández, M.; Pantanetti, M.; Viña, R.; Torriani, I.; Sánchez, R. M. T.; Punte, G. ODTMA + and HDTMA + organo-montmorillonites characterization: New insight by WAXS, SAXS and surface charge. *Appl. Clay Sci.* **2013**, *83−84*, 280−285.

(13) Suciu, N. A.; Ferrari, T.; Ferrari, F.; Trevisan, M.; Capri, E. Pesticide removal from waste spray-tank water by organoclay adsorption after field application: An approach for a formulation of cyprodinil containing antifoaming/defoaming agents. *Environ. Sci. Pollut. Res.* **2012**, *19*, 1229−1236.

(14) Magnoli, A. P.; Tallone, L.; Rosa, C. A. R.; Dalcero, A. M.; Chiacchiera, S. M.; Torres Sanchez, R. M. Commercial bentonites as detoxifier of broiler feed contaminated with aflatoxin. *Appl. Clay Sci.* **2008**, *40*, 63−71.

(15) Czímerová, A.; Bujdák, J.; Dohrmann, R. Traditional and novel methods for estimating the layer charge of smectites. *Appl. Clay Sci.* **2006**, *34*, 2−13.

(16) *PPDB: Pesticide Properties DataBase*; University of Hertfordshire: Hatfield, Hertfordshire, UK, 2011; http://sitem.herts.ac.uk/aeru/footprint/index2.htm.

(17) Sanchez-Martin, M. J.; Rodriguez-Cruz, M. S.; Andrades, M. S.; Sanchez-Camazano, M. Efficiency of different clay minerals modified with a cationic surfactant in the adsorption of pesticides: Influence of clay type and pesticide hydrophobicity. *Appl. Clay Sci.* **2006**, *31*, 216−228.

(18) Xu, S.; Boyd, S. A. Cationic surfactant adsorption by swelling and nonswelling layer silicates. *Langmuir.* **1995**, *11*, 2508−2514.

(19) Lee, S. Y.; Cho, W. J.; Hahn, P. S.; Lee, M.; Lee, Y. B.; Kim, K. J. Microstructural changes of reference montmorillonites by cationic surfactants. *Appl. Clay Sci.* **2005**, *30*, 174−180.

(20) Jiang, J.; Ai, L.; Li, L. Synthesis and characterization of polyaniline-based nanocomposites containing magnetic Li−Ni−La ferrite. *J. Non-cryst. Solids* **2009**, *355*, 1733−1736.

(21) Osman, M. A.; Ploetze, M.; Skrabal, P. Structure and properties of alkylammonium monolayers self-assembled on montmorillonite platelets. *J. Phys. Chem. B* **2004**, *108*, 2580−2588.

(22) Tong, D. S.; Zhou, C. H.; Lu, Y.; Yu, H.; Zhang, G. F.; Yu, W. H. Adsorption of Acid Red G dye on octadecyl trimethylammonium montmorillonite. *Appl. Clay Sci.* **2010**, *50*, 427−431.

(23) Madejová, J.; Jankovič, L.; Pentrák, M.; Komadel, P. Benefits of near-infrared spectroscopy for characterization of selected organo-montmorillonites. *Vib. Spectrosc.* **2011**, *57*, 8−14.

(24) Bishop, J. L.; Pieters, C. M.; Edwards, J. O. Infrared spectroscopic analyses on the nature of water in montmorillonite. *Clays Clay Miner.* **1994**, *42*, 702−716.

(25) Madejová, J.; Komadel, P. Baseline studies of the clay minerals society source clays: Infrared methods. *Clays Clay Miner.* **2001**, *49*, 410−432.

(26) Emmerich, K.; Plötze, M.; Kahr, G. Reversible collapse and Mg^{2+} release of de- and rehydroxylated homoionic cis-vacant montmorillonites. *Appl. Clay Sci.* **2001**, *19*, 143−154.

(27) Brindley, G. W.; Moll, W. F. Complexes of natural and synthetic Ca-montmorillonites with fatty acids. *Am. Mineral.* **1965**, *50*, 1355−1370.

(28) Zanini, G. P.; Ovesen, R. G.; Hansen, H. C. B.; Strobel, B. W. Adsorption of the disinfectant benzalkonium chloride on montmorillonite. Synergistic effect in mixture of molecules with different chain lengths. *J. Environ. Manage.* **2013**, *128*, 100−105.

(29) Zhu, J.; He, H.; Guo, J.; Yang, D.; Xie, X. Arrangement models of alkylammonium cations in the interlayer of HDTMA + pillared montmorillonites. *Chin. Sci. Bull.* **2003**, *48*, 368−372.

(30) Baldassari, S.; Komarneni, S.; Mariani, E.; Villa, C. Microwave versus conventional preparation of organoclays from natural and synthetic clays. *Appl. Clay Sci.* **2006**, *31*, 134−141.

(31) Thomas, F.; Michot, L. J.; Vantelon, D.; Montargès, E.; Prélot, B.; Cruchaudet, M.; Delon, J. F. Layer charge and electrophoretic mobility of smectites. *Colloids Surf., A* **1999**, *159*, 351−358.

(32) Miller, S. E.; Low, P. F. Characterization of the electrical double layer of montmorillonite. *Langmuir.* **1990**, *6*, 572−578.

(33) Pecini, E. M.; Avena, M. J. Measuring the isoelectric point of the edges of clay mineral particles: The case of montmorillonite. *Langmuir.* **2013**, *29*, 14926−14934.

(34) Praus, P.; Turicová, M.; Študentová, S.; Ritz, M. Study of cetyltrimethylammonium and cetylpyridinium adsorption on montmorillonite. *J. Colloid Interface Sci.* **2006**, *304*, 29−36.

(35) Li, Y.; Ishida, H. Concentration-dependent conformation of alkyl tail in the nanoconfined space: Hexadecylamine in the silicate galleries. *Langmuir.* **2003**, *19*, 2479−2484.

(36) Vazquez, A.; López, M.; Kortaberria, G.; Martín, L.; Mondragon, I. Modification of montmorillonite with cationic surfactants. Thermal and chemical analysis including CEC determination. *Appl. Clay Sci.* **2008**, *41*, 24−36.

(37) Xi, Y.; Frost, R. L.; He, H. Modification of the surfaces of Wyoming montmorillonite by the cationic surfactants alkyl trimethyl, dialkyl dimethyl, and trialkyl methyl ammonium bromides. *J. Colloid Interface Sci.* **2007**, *305*, 150−158.

(38) Park, Y.; Ayoko, G. A.; Frost, R. L. Characterisation of organoclays and adsorption of *p*-nitrophenol: Environmental application. *J. Colloid Interface Sci.* **2011**, *360*, 440−456.

(39) Socías-Viciana, M. M.; Hermosin, M. C.; Cornejo, J. Removing prometrone from water by clays and organic clays. *Chemosphere.* **1998**, *37*, 289−300.

(40) Hermosin, M. C.; Roldan, I.; Cornejo, J. Binding mechanisms of maleic hydrazide to homoionic montmorillonites. *Sci. Tatal Environ.* **1992**, *123−124*, 109−119.

(41) Celis, R.; Cornejo, J.; Hermosín, M. C.; Koskinen, W. C. Sorption-desorption of atrazine and simazine by model soil colloidal components. *Soil Sci. Soc. Am. J.* **1997**, *61*, 436−443.

(42) Jaynes, W. F.; Boyd, S. A. Hydrophobicity of siloxane surfaces in smectites as revealed by aromatic hydrocarbon adsorption from water. *Clays Clay Miner.* **1991**, *39*, 428−436.

(43) Laird, D. A. Interactions between atrazine and smectite surfaces. *ACS Symp. Ser.* **1996**, *630*, 85−100.

(44) Zhang, Y.; Zhao, Y.; Zhu, Y.; Wu, H.; Wang, H.; Lu, W. Adsorption of mixed cationic-nonionic surfactant and its effect on bentonite structure. *J. Environ. Sci.* **2012**, *24*, 1525−1532.

(45) Jing, P.; Hou, M.; Zhao, P.; Tang, X.; Wan, H. Adsorption of 2-mercaptobenzothiazole from aqueous solution by organo-bentonite. *J. Environ. Sci. Chin.* **2013**, *25*, 1139−1144.

(46) Yariv, S. IR spectroscopy and Thermo-IR spectroscopy in the study of the fine structure of organo-clay complexes. In *Organo-Clay Complexes and Interactions*; Yariv, S.; Cross, H., Eds.; Marcel Dekker, Inc: New York, 2001; pp 345−462.

(47) Yoshioka, N.; Akiyama, Y.; Teranishi, K. Rapid simultaneous determination of *o*-phenylphenol, diphenyl, thiabendazole, imazalil and its major metabolite in citrus fruits by liquid chromatography—mass spectrometry using atmospheric pressure photoionization. *J. Chromatogr.* **2004**, *1022*, 145−150.

(48) Kowalska, M.; Guler, H.; Cocke, D. L. Interactions of clay minerals with organic pollutants. *Sci. Total Environ.* **1994**, *141*, 223−240.